

Block encoding of matrix product operators

Martina Nibbi^{1,*} and Christian B. Mendl^{1,2,†}

¹*Technical University of Munich, School of CIT,*

Department of Computer Science, Boltzmannstraße 3, 85748 Garching, Germany

²*Technical University of Munich, Institute for Advanced Study, Lichtenbergstraße 2a, 85748 Garching, Germany*

Quantum signal processing combined with quantum eigenvalue transformation has recently emerged as a unifying framework for several quantum algorithms. In its standard form, it consists of two separate routines: block encoding, which encodes a Hamiltonian in a larger unitary, and signal processing, which achieves an almost arbitrary polynomial transformation of such a Hamiltonian using rotation gates. The bottleneck of the entire operation is typically constituted by block encoding and, in recent years, several problem-specific techniques have been introduced to overcome this problem. Within this framework, we present a procedure to block-encode a Hamiltonian based on its matrix product operator (MPO) representation. More specifically, we encode every MPO tensor in a larger unitary of dimension $D + 2$, where $D = \lceil \log(\chi) \rceil$ is the number of subsequently contracted qubits that scales logarithmically with the virtual bond dimension χ . Given any system of size L , our method requires $L + D$ ancillary qubits in total, while the number of one- and two-qubit gates decomposing the block encoding circuit scales as $\mathcal{O}(L \cdot \chi^2)$.

I. INTRODUCTION

Quantum signal processing (QSP) combined with “qubitization” provides a unifying paradigm for several quantum algorithms [1–4]. The quantum eigenvalue transformation (QET) technique is part of this framework. It facilitates a tailored polynomial transformation of the eigenvalues of a Hermitian matrix, which is typically a Hamiltonian \mathcal{H} of a quantum system of interest. QET has versatile applications, like eigenspace filtering, ground state preparation, and Hamiltonian simulation.

In this process, the most significant bottleneck is represented by the block encoding of \mathcal{H} . It is well known that a unitary operator embedding \mathcal{H} exists. However, decomposing such a unitary efficiently into one- and two-qubit gates requires some extra knowledge of the system and problem-specific techniques. In this context, we propose a versatile block encoding method based on a matrix product operator (MPO) representation of \mathcal{H} , where such an MPO form is typically known or can be constructed for systems of interest. Our method uses unitary dilations of the individual MPO tensors. Our approach achieves a block encoding with computational cost scaling only linearly with the system size L and quadratically with the virtual bond dimension χ of the MPO, while the number of ancillary qubits scales like the sum of L and $\log(\chi)$.

Our theoretical justification starts then in section II, where we provide a concise definition of MPOs within the context of tensor networks. This quick introduction is followed by the description of our algorithm in section III, which encodes such MPOs on a quantum computer. This task requires the use of ancillaries and measurements, as the MPO tensors are non-unitary in general.

We discuss the application of our method for QET in section IV and, specifically, we outline two methods to implement the signal processing operator: the original one described by Martyn et al. [3] and an alternative that requires no auxiliary qubits. The theoretical proof of the correctness of this method is provided in appendix A.

We then perform a cost analysis in terms of two-qubit gates count, comparing our method to the linear combinations of unitaries (LCU) block encoding technique in section V. The results show that our technique is characterized by a scaling of $\mathcal{O}(L \cdot \chi^2)$, while the cost of LCU varies depending on the number of unitaries composing the Hamiltonian.

Finally, we present some practical applications in section VI. We examine the MPO representation of the Ising and Heisenberg Hamiltonians and an exponentially decaying XY model, which exhibits a significant advantage compared to the use of LCU. We also consider a general tensor product of sums of Paulis as a straightforward example for realizing the entire QET circuit simulating an eigenstate filtering process.

II. TENSOR NETWORKS AND MATRIX PRODUCT OPERATORS

We consider a physical system that can be represented as a one-dimensional chain with L sites. Then, a matrix product operator (MPO) is any operator acting on such a system as [5, 6]:

$$O = \tilde{A}^{(1)} A^{(2)} A^{(3)} \dots A^{(L-1)} \tilde{A}^{(L)} \quad (1)$$

where every term $A^{(\ell)}$ is a matrix of operators acting on the ℓ -th site of the lattice except for the first and last term, which are respectively a row and column vector of operators. For concreteness, we will assume that the MPO has uniform virtual bond dimension χ and physical wires of dimension 2. Other scenarios follow by a straightforward generalization.

* martina.nibbi@tum.de

† christian.mendl@tum.de

Figure 1a represents the tensor diagram of Eq. (1). In Fig. 1b, we defined the boundary tensors $\tilde{A}^{(1)}$ and $\tilde{A}^{(L)}$ as the contraction between two tensors $A^{(1)}$ and $A^{(L)}$ of degree four, respectively with a row and column vector R and C . Such a manipulation of the boundary tensors conveniently allows us to work with an MPO with uniform dimensions, while the role of the vectors R and C will be further investigated in sections IV and VI.

Such a decomposition can always be found through iterated singular values decompositions, exactly like matrix product states (MPS) [5]. However, this method quickly becomes computationally too expensive for increasing L , so it is considered impracticable for most applications. Instead, it is possible to build the MPO by representing the Hamiltonian through finite state automata [7, 8]. This method is particularly suitable for translation-invariant systems. We will show a few examples in section VI. From now on, we will assume that the MPO decomposition of the target Hamiltonian is known.

III. CIRCUIT REPRESENTATION

Now that the basic concepts for understanding matrix product operators have been introduced, we describe how to implement them on a quantum circuit. First of all, to make the tensors $A^{(\ell)}$ act on qubits as a quantum gate, we need to reshape them from four-tensors to matrices as shown below:

$$\text{Diagram showing the reshaping of a four-legged tensor } A^{(\ell)} \text{ into a matrix } \mathcal{M}[A^{(\ell)}].$$

where we define $\mathcal{M}[A^{(\ell)}]$ as the matrix reshape of the tensor $A^{(\ell)}$.

Given then the virtual bond dimension of the original MPO χ , which we assumed to be uniform, we proceed to expand the matrices $\mathcal{M}[A^{(\ell)}]$ so that their dimensions reach the next power of 2. Examples of this procedure will be shown in the applications section. Then, since we have postulated the physical wire to have dimension 2, we can assume $\mathcal{M}[A^{(\ell)}]$ to have dimensions $2^{D+1} \times 2^{D+1}$, where D is defined as:

$$D = \lceil \log(\chi) \rceil \quad (2)$$

where the logarithm is intended in base 2. It should be clear that if the physical wire can be represented with one single qubit, the virtual bond needs D qubits. From now on, we will refer to the latter as *virtual bond ancillaries*.

The last step needed to represent $\mathcal{M}[A^{(\ell)}]$ as a quantum circuit is a unitary dilation, i.e., we embed each $\mathcal{M}[A^{(\ell)}]$ as a block in a larger unitary matrix. This procedure will require another ancillary qubit, which we will refer to as *dilation ancillary*. From a diagrammatic point of view, after reshaping the unitary matrices into tensors of degree 4, we get the final MPO form as in Fig. 1c. Here, each green wire corresponds to one physical qubit,

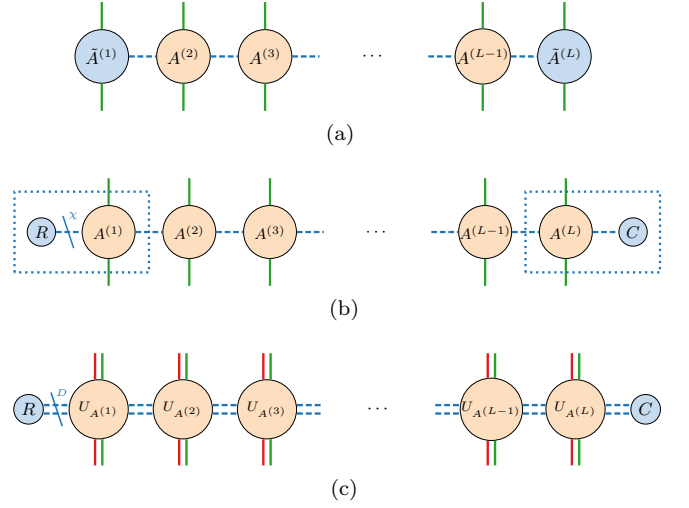


Figure 1. **1a**: Tensor diagram of a general matrix product operator with open boundary conditions. **1b**: The three-legged tensors $\tilde{A}^{(1)}$ and $\tilde{A}^{(L)}$ result from contracting the four-legged tensors $A^{(1)}$ and $A^{(L)}$ respectively with the row and column vectors R and C . **1c**: Unitary dilation of the $A^{(\ell)}$ tensors. The D virtual bond ancillaries are drawn in blue and dashed, the dilation ancillaries in red, and the physical qubits in green.

each red wire has the role of dilation ancillary, and the D blue dashed wires represent the virtual bond ancillaries.

Using one ancillary qubit has the effect of doubling the size of the encoding unitaries: more specifically, we want to define a unitary matrix $U_{A^{(\ell)}}$ so that its upper-left block is equal to $\mathcal{M}[A^{(\ell)}]$ up to a normalization factor N_ℓ :

$$U_{A^{(\ell)}} = \begin{pmatrix} \mathcal{M}[A^{(\ell)}]/N_\ell & C \\ B & D \end{pmatrix}. \quad (3)$$

We denote such unitaries as *block encodings* of the matrices $\mathcal{M}[A^{(\ell)}]$. Note that the normalization factor is necessary because $\mathcal{M}[A^{(\ell)}]$ is typically not normalized and is characterized by the relation:

$$N_\ell \geq \|\mathcal{M}[A^{(\ell)}]\|, \quad (4)$$

with $\|\cdot\|$ denoting the spectral norm. Our aim now is to find the blocks B , C and D so that, given $A^{(\ell)}$, $U_{A^{(\ell)}}$ is unitary. We rely on a similar procedure as proposed in [9, Appendix D].

1. From the unitary constraint on $U_{A^{(\ell)}}$ it follows that

$$B^\dagger B = I - \mathcal{M}[A^{(\ell)}]^\dagger \mathcal{M}[A^{(\ell)}]/N_\ell^2. \quad (5)$$

Let us consider then the singular value decomposition of the matrix $\mathcal{M}[A^{(\ell)}]$:

$$\mathcal{M}[A^{(\ell)}] = U \Sigma V^\dagger \quad (6)$$

with U and V unitary matrices and Σ the diagonal matrix of singular values.

By substituting Eq. (6) into Eq. (5) we get then:

$$B^\dagger B = V (I - \Sigma^2/N_\ell^2) V^\dagger. \quad (7)$$

The normalization factor ensures that the matrix $I - \Sigma^2/N_\ell^2$ is non-negative, so that we can identify:

$$B = \sqrt{I - \Sigma^2/N_\ell^2} V^\dagger. \quad (8)$$

2. Let us consider now the following rectangular matrix:

$$W = \begin{pmatrix} \mathcal{M}[A^{(\ell)}]/N_\ell \\ B \end{pmatrix} \quad (9)$$

where B has been found through the previous step. A full QR decomposition applied to W returns a unitary matrix U and a rectangular, upper triangular matrix R so that

$$W = UR. \quad (10)$$

In the first half of its columns, U will share the same entries as W , since they were already orthonormal; as a result, the unitary matrix U is of the form (3), so that we can set $U_{A^{(\ell)}} = U$.

Now that we have achieved a unitary block encoding for each $A^{(\ell)}$, we can represent the entire MPO tensor network by a quantum circuit. Fig. 2 shows the full block encoding circuit for a generic Hamiltonian \mathcal{H} acting on a system of size $L = 3$ as an example. Note that:

- The block encoding circuit needs in total L physical qubits, marked in green, D virtual bond ancillaries, blue dashed, and L dilation ancillaries, marked in red. The total number of ancillaries is then $L + D$, and the color scheme matches the one for the equivalent wires of the tensor networks in Fig 1.
- The encoded Hamiltonian \mathcal{H} is normalized by a factor $\prod_{\ell=1}^L N_\ell$.
- To retrieve \mathcal{H} , the dilation ancillaries must be all initialized and measured in the state $|0\rangle$. The virtual bond ancillaries must also be prepared in state $|C\rangle$ and measured in state $|R\rangle$, representing the column and row vectors C and R previously defined. As a result, a post-selection operation is needed to fully implement \mathcal{H} on a quantum circuit but, remarkably, the probability of measuring the right states is independent of the block encoding technique and number of ancillaries [10]:

$$\begin{aligned} p_{\text{success}} &= \|\langle 0| \otimes \langle R| U |C\rangle \otimes |0\rangle \otimes |\psi_{\text{in}}\rangle\|^2 \\ &= \left\| \frac{\mathcal{H}}{\prod_{\ell=1}^L N_\ell} |\psi_{\text{in}}\rangle \right\|^2 \\ &= \sum_k \left| \frac{\lambda_k}{\prod_{\ell=1}^L N_\ell} \right|^2 \cdot |\langle \lambda_k | \psi_{\text{in}} \rangle|^2 \end{aligned} \quad (11)$$

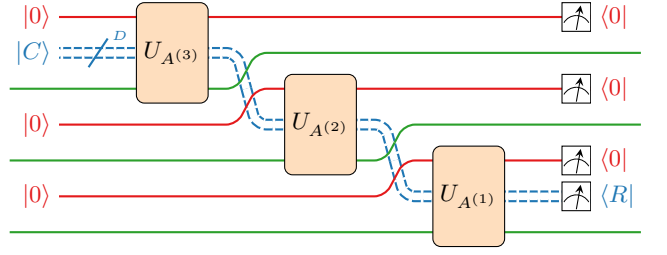


Figure 2. Quantum circuit implementing the MPO representation of a generic quantum Hamiltonian, illustrated for a system with $L = 3$ sites.

where $|\psi_{\text{in}}\rangle$ is the input state on the physical wires and we have used the eigendecomposition of H : $H = \sum_k \lambda_k |\lambda_k\rangle \langle \lambda_k|$. Interestingly enough, the probability is maximal when $|\psi_{\text{in}}\rangle$ has a big overlap with the eigenvector corresponding to the maximal eigenvalue. Note that the normalization factors will, in general, affect the success probability. This aspect will be further discussed in sections IV and VII.

- The cost for decomposing each $U_{A^{(\ell)}}$ into one- and two-qubit gates drastically varies for different applications and different native gate sets of the specific hardware. Nonetheless, in the most general case, it grows exponentially with the number of wires involved in each gate, equal to $D+2$, so that the number of two-qubit gates scales as $\mathcal{O}(L \cdot 4^D)$ [11, 12]. Returning to the virtual bond dimension formalism and recalling Eq. (2), we can conclude that the computational cost for the MPO circuit scales linearly with the system size and quadratically with the virtual bond dimension as $\mathcal{O}(L \cdot \chi^2)$.

IV. QUANTUM EIGENVALUE TRANSFORMATION WITH MPO BLOCK ENCODING

We now illustrate the quantum eigenvalue transformation (QET) algorithm [3] as a possible application of our block encoding method.

Given a block encoding U of a Hamiltonian \mathcal{H} and a polynomial of degree d , there exists a sequence of angles $\{\phi_k\}_{k=1,\dots,d}$ so that (in the case of d even):

$$\prod_{k=1}^{d/2} (\Pi_{\phi_{2k-1}} U^\dagger \Pi_{\phi_{2k}} U) = \begin{pmatrix} \text{Poly}_d(\mathcal{H}) & * \\ * & * \end{pmatrix}. \quad (12)$$

The signal processing operators Π_{ϕ_k} are defined as:

$$\Pi_{\phi_k} = e^{-i\phi_k(2|\Pi\rangle\langle\Pi| - I)} \quad (13)$$

where $|\Pi\rangle\langle\Pi|$ is the projector onto \mathcal{H} : $\langle\Pi|U|\Pi\rangle = \mathcal{H}$.

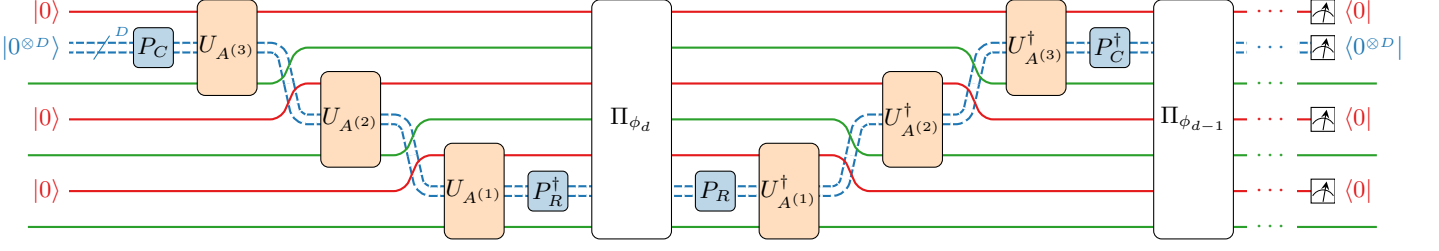


Figure 3. MPO block encoding in the quantum eigenvalue transformation circuit without specifying the signal processing gates.

Similarly, for odd d , Eq. (12) becomes:

$$\Pi_{\phi_1} U \prod_{k=2}^{(d-1)/2} (\Pi_{\phi_{2k}} U^\dagger \Pi_{\phi_{2k+1}} U) = \begin{pmatrix} \text{Poly}_d(\mathcal{H}) & * \\ * & * \end{pmatrix}. \quad (14)$$

In the previous sections, we have illustrated how to create a unitary encoding for an MPO Hamiltonian acting on L sites through $L + D$ ancillary qubits. To retrieve the Hamiltonian from $U_{A(\ell)}$ depicted in Fig. 2, we need to project onto $|0\rangle$ for all the red wires (both initialization and measurement), while for the virtual bond ancillaries we need to initialize the state $|C\rangle$ and measure $|R\rangle$. For the sake of simplicity, we make use of the two state-preparation gates P_C and P_R :

$$P_C |0 \cdots 0\rangle = |C\rangle \quad (15)$$

$$P_R |0 \cdots 0\rangle = |R\rangle \quad (16)$$

to initialize and measure the virtual bond ancillaries in the state $|0 \cdots 0\rangle$, just like the dilation ancillaries.

In section III, we have shown how the probability of success in the post-selection process doesn't depend on the block encoding technique or the number of ancillaries. A similar analysis can be done for the full QET circuit:

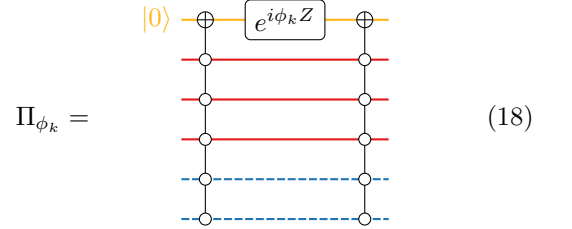
$$\begin{aligned} p_{\text{success}} &= \|\langle 0| \otimes \langle R| U_{\text{QET}} |C\rangle \otimes |0\rangle \otimes |\psi_{\text{in}}\rangle\|^2 \\ &= \left\| \text{Poly}_d \left(\frac{\mathcal{H}}{\prod_{\ell=1}^L N_\ell} \right) |\psi_{\text{in}}\rangle \right\|^2 \\ &= \sum_k \left| \text{Poly}_d \left(\frac{\lambda_k}{\prod_{\ell=1}^L N_\ell} \right) \right|^2 \cdot |\langle \lambda_k | \psi_{\text{in}} \rangle|^2 \end{aligned} \quad (17)$$

Remarkably, this time, the probability of success is maximal when $|\psi_{\text{in}}\rangle$ has a big overlap with the eigenvector $|\lambda_k\rangle$ corresponding to the largest eigenvalue (in magnitude) after the transformation, and not of the original Hamiltonian. Note also that the normalization factors do not directly suppress the success probability anymore because they now appear in the argument of the polynomial transformation. Further discussion about this topic can be found in section VII.

The overall QET circuit, before specifying how to build the signal processing operator, is visualized in Fig. 3.

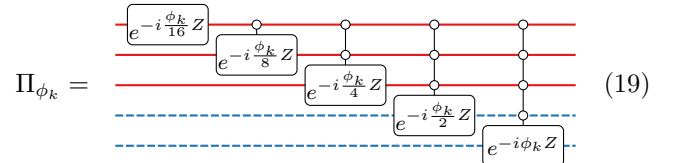
Martyn et al.'s paper [3] contains a first proposal for building the operator Π_{ϕ_k} with one extra auxiliary qubit.

As an example, the mentioned operator would be implemented in the following way for $L = 3$ and $D = 2$:



Note that we always need exactly one extra auxiliary qubit (in yellow), and the signal processing gate acts on all the dilation and virtual bond ancillaries. Decomposing the two Toffolis requires then $\mathcal{O}((L+D)^2)$ one- and two-qubit gates, or even $\mathcal{O}(L+D)$ if we allow a second extra ancillary [13, 14].

Here we suggest a possible alternative approach to implement Π_{ϕ_k} using multi-controlled Z-rotations, instead of multi-controlled NOTs, and no extra auxiliary qubit. For the same example as in Eq. (18), the circuit reads (see Appendix A for a derivation):



where the n -th gate is controlled by $n-1$ qubits and the corresponding Z-rotation has phase $\frac{\phi}{2^{L+D-n}}$.

An $SU(2)$ multi-controlled single-qubit unitary can be decomposed in one- and two-qubit elementary gates with only a linear scaling and no extra ancillaries [15]. By summing all the controlled rotations, we retrieve then a quadratic computational complexity, which matches the first circuit if decomposed without any other ancillary.

Note that the cascading shape of our MPO block encoding allows part of the signal processing circuit to be executed in parallel with the block encoding, with a further reduction of the circuit's depth, as illustrated in Fig. 4. Given the interchangeability of the ancillaries from the signal processing point of view, we can invert the order of the controlled rotations and start from the bottom wire up, so that also U^\dagger can be partially executed in parallel with the following Π_{ϕ_k} .

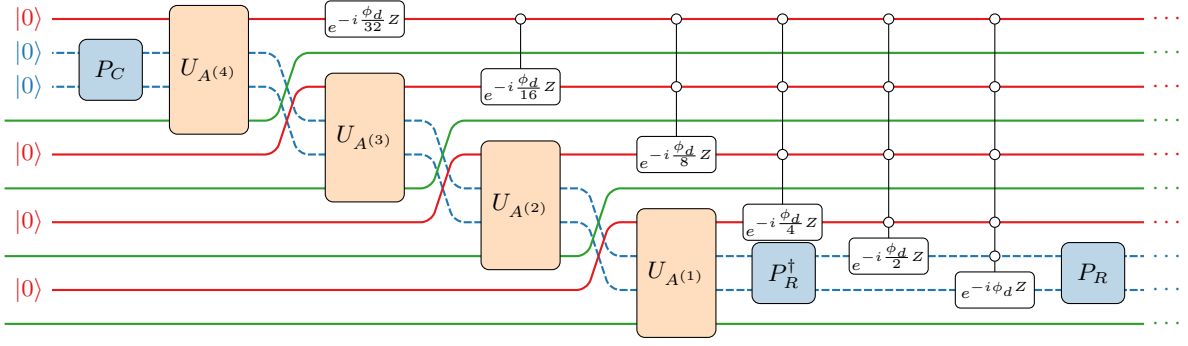


Figure 4. First QET step with $L = 4$ and $D = 2$. If the Hamiltonian acts on L particles, the first $L - 1$ terms of the signal processing circuit can be executed in parallel with the block encoding.

This decomposition could be practical for devices that have controlled phase rotations instead of cNOTs as native gates. However, it could present a worse scaling if we allow for extra ancillaries. We are then leaving the choice for the signal processing implementation open since many factors have to be taken into account.

V. COST ANALYSIS

Before illustrating some possible applications, we would like to discuss the cost of a general QET circuit built with our block encoding algorithm, in comparison to the linear combination of unitaries (LCU) technique [2, 16, 17] shown in Fig. 5. More specifically, we evaluate the computational cost based on the count of one- and two-qubit gates.

The LCU method is based on the insight that every Hamiltonian can be written as a linear combination of unitaries:

$$\mathcal{H} = \sum_{m=1}^M \alpha_m U_m. \quad (20)$$

For concreteness, we will consider the case where all the U_M are Pauli strings. The total number of terms in the summation is denoted as M . In the worst case scenario, M scales exponentially with the system size L as

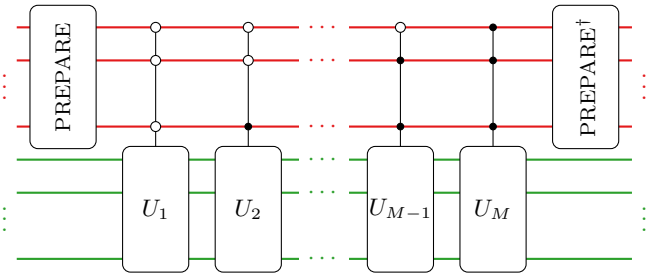


Figure 5. Linear combination of unitaries block encoding technique

$M = \mathcal{O}(4^L)$. Still, there are important examples of polynomial or even linear scaling, like the Ising or Heisenberg Hamiltonian. We will first discuss the general case and then return to the specific examples later.

For LCU, one first adds $\lceil \log(M) \rceil$ ancillary qubits to the circuit that need to be prepared in the state:

$$|\text{PREP}\rangle = \sum_{m=1}^M \alpha_m |m\rangle \quad (21)$$

with the same coefficients α_m as in Eq. (20). This preparation gate, as well as any other multi-qubit controlled gate that we will consider in this section, must be decomposed into one- and two-qubit gates. Generally speaking, this process has a cost that scales exponentially with the number of qubits [19], which means $\mathcal{O}(M)$.

The next step is known as the selection phase: here, each state $|m\rangle$ controls one of the unitaries U_m . We have therefore M Pauli strings acting on the L system qubits and controlled by the $\lceil \log(M) \rceil$ ancillary qubits. Supposing that each Pauli gate can be implemented with a constant cost on a quantum computer, we get $\mathcal{O}(L)$ terms for each U_m . Then, for the decomposition of each multi-controlled Pauli, we have two possible choices:

1. No extra auxiliaries, which brings a quadratic cost in the number of controls [18].
2. One extra auxiliary qubit each, which allows for a linear scaling with the number of controls [14]. Note that the cited work refers to a n -controlled NOT, which can easily be converted into a multi-controlled Z or Y gate with constant cost. Assuming that the new extra qubit is entangled with the system and cannot be reused, in total this requires $L \cdot M$ extra auxiliaries for each U and U^\dagger in the QET circuit.

As a consequence, the cost of the decomposition for the full selection phase scales as $\mathcal{O}(L \cdot M \cdot \log^\alpha(M))$, where α is equal to 1 or 2 based on the presence of extra auxiliaries.

As a last step, we need to apply the inverse preparation gate on the ancillaries, with a final cost of $\mathcal{O}(2M + L \cdot M \cdot \log^\alpha(M)) = \mathcal{O}(L \cdot M \cdot \log^\alpha(M))$.

	Block encoding ancillary qubits	Block encoding computational cost (no extra auxiliaries)	Martyn et al. [3] signal processing computational cost (1 extra auxiliary)
MPO Block Encoding	$L + D$	$\mathcal{O}(L \cdot \chi^2)$	$\mathcal{O}(L + \log(\chi))$
LCU Block Encoding	$\lceil \log(M) \rceil$	$\mathcal{O}(L \cdot M \cdot \log^2(M))$	$\mathcal{O}(\log(M))$
LCU Block Encoding $M = \mathcal{O}(L)$	$\mathcal{O}(\log(L))$	$\mathcal{O}(L^2 \cdot \log^2(L))$	$\mathcal{O}(\log(L))$
LCU Block Encoding $M \simeq 4^L$	$2L$	$\mathcal{O}(L^3 \cdot 4^L)$	$\mathcal{O}(L)$

Table I. Cost comparison between the LCU and MPO block encoding and signal processing in terms of number of single- and two-qubit gates and encoding ancillaries. The analysis assumes a cost for decomposing a general unitary on n qubits of $\mathcal{O}(4^n)$ [11, 12]. For the block encodings, we decompose multi-controlled Pauli gates with a quadratic cost without the use of extra auxiliary qubits [13, 18]. We consider Martyn et al.’s signal processing implementation [3] and a linear n -Toffoli decomposition which makes use of 1 extra auxiliary qubit [15]. The number of bond ancillary qubits D scales logarithmically with respect to the MPO virtual bond dimension χ as $D = \lceil \log(\chi) \rceil$.

Considering now some special cases:

- In the worst-case scenario, with M scaling as 4^L , we get $\mathcal{O}(L)$ encoding ancillary qubits and a total cost of $\mathcal{O}(L^{1+\alpha} \cdot 4^L)$ gates. The case $\alpha = 1$ would also require $\mathcal{O}(L \cdot 4^L)$ extra auxiliaries.
- For a general linear scaling, we get a total cost for the decomposition of $\mathcal{O}(L^2 \cdot \log^\alpha(L))$ with only $\mathcal{O}(\log(L))$ encoding ancillaries and $\mathcal{O}(L^2)$ optional extra auxiliaries for the decomposition for $\alpha = 1$.
- The aforementioned Ising and Heisenberg Hamiltonians also present a linear scaling, since they are defined as a linear sum of Pauli strings. However, because of the nearest-neighbor constraint, they can get even better complexity of $\mathcal{O}(L \cdot \log^\alpha(L))$, as the Pauli strings U_m are only composed by one or two Pauli gates, and $\mathcal{O}(L)$ optional extra auxiliaries for the decomposition for $\alpha = 1$.

We notice that adding extra auxiliaries in this framework brings a limited advantage compared to their scaling. For this reason, from now on we will only consider the case of no extra auxiliaries allowed for the decomposition of multi-controlled gates in the LCU block encoding.

Regarding our MPO block encoding, we will only consider its worst-case scenario. The resulting circuit shown in Fig. 2 is implemented through L unitaries acting each on $D + 2$ wires: decomposing them requires a cost of $\mathcal{O}(L \cdot 4^D) = \mathcal{O}(L \cdot \chi^2)$ at most. The preparation gates P_C and P_R do not change the formal complexity, as they scale at most as $\mathcal{O}(\chi)$ [19]. In conclusion, we can state that we always get a linear dependence on the system size L and a quadratic scaling with the virtual bond dimension χ . It is also worth recalling that the number of ancillary qubits is precisely equal to $L + D$.

Table I summarizes the MPO and LCU block encoding costs, the latter with specific examples of M scaling exponentially or linearly with L . We also added the signal processing decomposition cost, which scales only linearly with the number of ancillary qubits if we consider Martyn et al.’s implementation [3] and one extra auxiliary qubit [15].

Given the linear scaling with L and the quadratic dependence on χ , our block encoding turns out to be competitive compared to LCU. If we consider, for example, the aforementioned Ising and Heisenberg models, the corresponding MPO block encoding scales only linearly with L since χ is constant, as it will be further discussed in section VI with other applications.

On the other hand, the relatively large number of ancillary qubits can make the signal processing phase more expensive. However, considering the entire QET circuit, we can conclude that this typically doesn’t constitute a limitation since the block encoding still prevails in the overall computational cost. The post-selection, moreover, is not affected by the number of ancillaries, as we have shown in Eq. (17).

In conclusion, our method can constitute a valid alternative to LCU from a circuit size point of view. The two techniques are not directly comparable because M and χ have different dependencies on the system size based on the application. We will show some example applications in section VI.

It is also worth mentioning that this analysis is based on the current technologies not allowing three-qubit gates (or more), and future hardware developments, as well as better multi-controlled unitaries’ decomposition techniques, might revise this analysis.

VI. APPLICATIONS

This section demonstrates how our block encoding technique can be applied to specific Hamiltonians. As a first example, we consider the Ising and Heisenberg Hamiltonians, which have a relatively simple MPO representation, and a slightly modified version of the XY model with exponentially decaying potential.

Then, we consider the case where a sum of Pauli strings can be rearranged in a tensor product of sums of local Pauli operators. For this system, we also perform an eigenstate filtering procedure through an entire QET circuit.

A. Ising model with transverse field

The Ising Hamiltonian with transverse field is defined as follows:

$$\mathcal{H}_{\text{Ising}} = J \sum_{\ell=1}^{L-1} Z_{\ell} Z_{\ell+1} + g \sum_{\ell=1}^L X_{\ell} \quad (22)$$

with Z_{ℓ} and X_{ℓ} Pauli operators acting on the ℓ -th site. Then, a suitable MPO decomposition can be achieved by defining the internal $A^{(\ell)}$ tensors as [7, 20]:

$$A^{(\ell)} = \begin{pmatrix} I_{\ell} & 0 & 0 \\ Z_{\ell} & 0 & 0 \\ gX_{\ell} & JZ_{\ell} & I_{\ell} \end{pmatrix} \quad (23a)$$

and by “closing” the tensor chain with the following initial and final vectors of operators, respectively:

$$\tilde{A}^{(1)} = (gX_1 \ JZ_1 \ I_1), \quad (23b)$$

$$\tilde{A}^{(L)} = \begin{pmatrix} I_L \\ Z_L \\ gX_L \end{pmatrix}. \quad (23c)$$

Every local operator O_{ℓ} acts on the ℓ -th lattice site, and I is the 2×2 identity matrix. Such a representation can be easily found through a finite state automata picture of the Hamiltonian, as shown in [7, 16].

One can also verify that the boundary vectors can be obtained via:

$$(gX_1 \ JZ_1 \ I) = (0 \ 0 \ I) \cdot A^{(1)}, \quad (24a)$$

$$\begin{pmatrix} I \\ Z_L \\ gX_L \end{pmatrix} = A^{(L)} \cdot \begin{pmatrix} I \\ 0 \\ 0 \end{pmatrix} \quad (24b)$$

with $A^{(1)}$ and $A^{(L)}$ defined as the other $A^{(\ell)}$. Eq. (1) for the Ising model then becomes:

$$\mathcal{H}_{\text{Ising}} = (0 \ 0 \ I) \left[\prod_{\ell=1}^L \begin{pmatrix} I & 0 & 0 \\ Z_{\ell} & 0 & 0 \\ gX_{\ell} & JZ_{\ell} & I \end{pmatrix} \right] \begin{pmatrix} I \\ 0 \\ 0 \end{pmatrix}. \quad (25)$$

We immediately notice that since the Pauli operators act on single qubits, and have dimension 2×2 , each matrix has dimension 6×6 and therefore needs at least 3 qubits to be represented. As a consequence, all the matrices and vectors in Eq. (25) gain a new row and/or column in the following way:

$$R \longrightarrow (0 \ 0 \ 1 \ 0) = \langle 10|, \quad (26a)$$

$$C \longrightarrow \begin{pmatrix} 1 \\ 0 \\ 0 \\ 0 \end{pmatrix} = |00\rangle, \quad (26b)$$

$$A^{(\ell)} \longrightarrow \begin{pmatrix} I & 0 & 0 & 0 \\ Z_{\ell} & 0 & 0 & 0 \\ gX_{\ell} & JZ_{\ell} & I & 0 \\ 0 & 0 & 0 & I \end{pmatrix}. \quad (26c)$$

The state-preparation gates P_C and P_R are the identity operator and $X \otimes I$, respectively.

Among the 3 qubits that represent each matrix $A^{(\ell)}$, only one has the role of physical qubit (different for every tensor), while the other 2 are subsequently contracted. Moreover, the meaning of the column and row vectors C and R is now clearer, as they correspond to the initialization of the virtual bond ancillaries in the state $|00\rangle$ and their projection after measurement in the state $|10\rangle$.

Note that to construct a block encoding of $A^{(\ell)}$, we have to normalize it by a factor $N \geq \|\mathcal{M}[A^{(\ell)}]\|$. This has the same effect as dividing the Hamiltonian parameters J and g by N^L :

$$J \longrightarrow \frac{J}{N^L}, \quad (27a)$$

$$g \longrightarrow \frac{g}{N^L}. \quad (27b)$$

It is worth mentioning that some algorithms, including the eigenstate filtering process that we have applied to the tensor product of Pauli sums, require the eigenvalues of \mathcal{H} not only to have an absolute value smaller than 1, but also to be positive. To achieve that, one may add an extra auxiliary qubit and control the entire block encoding process as shown in Fig. 6 [3]. Within our specific technique, however, we can add a term ζI to Eq. (22) without any extra computational cost by simply changing the MPO definition and initial and final projections:

$$|R\rangle \longrightarrow \frac{1}{\sqrt{2}} (0 \ 0 \ 1 \ 1) = \frac{\langle 10| + \langle 11|}{\sqrt{2}} \quad (28a)$$

$$|C\rangle \longrightarrow \frac{1}{\sqrt{2}} \begin{pmatrix} 1 \\ 0 \\ 0 \\ 1 \end{pmatrix} = \frac{|00\rangle + |11\rangle}{\sqrt{2}} \quad (28b)$$

$$A^{(\ell)} \longrightarrow \begin{pmatrix} I & 0 & 0 & 0 \\ Z_{\ell} & 0 & 0 & 0 \\ gX_{\ell} & JZ_{\ell} & I & 0 \\ 0 & 0 & 0 & \zeta^{1/L} I \end{pmatrix} \quad (28c)$$

As a consequence, the state preparation operators become:

$$P_R = \text{---} \boxed{H} \text{---} \quad (29a)$$

$$P_C = \text{---} \boxed{H} \text{---} \bullet \oplus \quad (29b)$$

Note that, when normalizing the Hamiltonian, we also need to consider an extra factor 2 given by the normalization of states $|R\rangle$ and $|C\rangle$, so that:

$$J \longrightarrow \frac{J}{2N^L}, \quad (30a)$$

$$g \longrightarrow \frac{g}{2N^L}. \quad (30b)$$

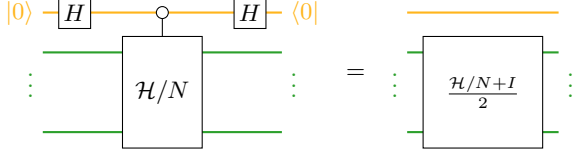


Figure 6. One possible strategy for shifting the eigenvalues of \mathcal{H} from the interval $[-1, 1]$ to $[0, 1]$ that works for every block encoding strategy.

In the specific Ising case, we can thus shift the eigenvalues of \mathcal{H} in the interval $[0, 1]$ without a significant increase in the computational cost. In other cases, however, adding a new identity operator in the right-bottom corner of $A^{(\ell)}$ could increase the dimension beyond 2^D , requiring one additional virtual bond ancillary.

B. Heisenberg model

Next, we discuss the Heisenberg model governed by the Hamiltonian

$$\begin{aligned} \mathcal{H}_{\text{Heis}} = & \sum_{\ell=1}^{L-1} (J_X X_\ell X_{\ell+1} + J_Y Y_\ell Y_{\ell+1} + J_Z Z_\ell Z_{\ell+1}) \\ & + \sum_{\ell=1}^L (g_X X_\ell + g_Y Y_\ell + g_Z Z_\ell). \end{aligned} \quad (31)$$

It can be proven that the corresponding MPO decomposition has a similar structure as for the Ising model with matrices $A^{(\ell)}$ [7, 21]:

$$A^{(\ell)} = \begin{pmatrix} I & 0 & 0 & 0 & 0 \\ X_\ell & 0 & 0 & 0 & 0 \\ Y_\ell & 0 & 0 & 0 & 0 \\ Z_\ell & 0 & 0 & 0 & 0 \\ g_X X_\ell + g_Y Y_\ell + g_Z Z_\ell & J_X X_\ell & J_Y Y_\ell & J_Z Z_\ell & I \end{pmatrix}. \quad (32)$$

The matrix $A^{(\ell)}$ in Eq. (32) has dimension 10×10 and therefore needs to be expanded into a 16×16 matrix (analogous to the Ising MPO model) to be represented by 4 qubits. Moreover, another dilation ancillary is added to build $U_{A^{(\ell)}}$ through a QR decomposition.

As a result, the entire block encoding circuit resembles the Ising example but with 3 virtual bond ancillaries instead of 2, given the larger dimensions of $A^{(\ell)}$; the latter needs then to be initialized in the state $|000\rangle$ and measured in the state $|101\rangle$.

C. Exponentially decaying XY model

The XY model, which restricts the more general Heisenberg model to the XY plane, is particularly inter-

esting. Removing the 2 rows and columns containing Z_ℓ results in an MPO matrix of dimensions 8×8 , which can be represented with 3 qubits and no further expansion. Thus, the XY model requires the same computational resources as the Ising model.

Here, more specifically, we will consider a slightly different version of this model, where we will relax the nearest neighbor assumption with an exponentially decaying interaction (and no transverse field, for simplicity):

$$\mathcal{H}_{\text{XY}_\alpha} = \sum_{\ell_1=1}^L \sum_{\ell_2=\ell_1+1}^L e^{-\alpha|\ell_1-\ell_2|} (J_X X_{\ell_1} X_{\ell_2} + J_Y Y_{\ell_1} Y_{\ell_2}) \quad (33)$$

with $\alpha > 0$.

If we wanted to represent such a Hamiltonian with a linear combination of unitaries, we would need to consider $M = \mathcal{O}(L^2)$ terms, which results in a computational complexity of $\mathcal{O}(L^2 \cdot \log^2(L))$ and $\mathcal{O}(\log(L))$ ancillaries.

On the other hand, this model has a very simple MPO representation with the same virtual bond dimension as the standard XY model $\chi = 4$ [6]:

$$A^{(\ell)} = \begin{pmatrix} I & 0 & 0 & 0 \\ e^{-\alpha} X_\ell & e^{-\alpha} I & 0 & 0 \\ e^{-\alpha} Y_\ell & 0 & e^{-\alpha} I & 0 \\ 0 & J_X X_\ell & J_Y Y_\ell & I \end{pmatrix}. \quad (34)$$

Our MPO block encoding technique would then be able to represent this Hamiltonian with a number of one- and two-qubit scaling only linearly with the system size L . The number of ancillaries would also scale as $\mathcal{O}(L)$ as well as the cost of the signal processing, giving a total cost for a full QET circuit of only $\mathcal{O}(d \times L)$, where d is the degree of the polynomial. It's also worth noticing that we don't need to consider exponentially decaying coefficients, as the factor $e^{-\alpha}$ is the same in every matrix $A^{(\ell)}$.

We have then found a first example of a practical application where our technique can constitute a significant advantage compared to the previous state-of-the-art method.

D. Tensor product of sum of Paulis

Finally, we consider a different Hamiltonian on which we test the entire QET algorithm by applying an eigenstate filtering transformation. Let us consider the particular case of a tensor product of sums of local Pauli matrices:

$$\mathcal{H}_{\text{TP}} = \bigotimes_{\ell=1}^L (\alpha_\ell I + \beta_\ell X_\ell + \gamma_\ell Y_\ell + \delta_\ell Z_\ell). \quad (35)$$

The MPO representation is straightforward, as each MPO tensor is a one-qubit matrix:

$$A^{(\ell)} = (\alpha_\ell I + \beta_\ell X_\ell + \gamma_\ell Y_\ell + \delta_\ell Z_\ell) \quad (36)$$

with $D = 0$ virtual bond ancillaries.

Following the eigenstate filtering process from Martyn et al.'s paper [3], we learn that the Hamiltonian should only have positive eigenvalues. By following a similar strategy as discussed for the Ising model, we add an element ζI to \mathcal{H}_{TP} ; the tensors $A^{(\ell)}$ are then modified in the following way:

$$A^{(\ell)} \longrightarrow \begin{pmatrix} \alpha_\ell I + \beta_\ell X_\ell + \gamma_\ell Y_\ell + \delta_\ell Z_\ell & 0 \\ 0 & \zeta^{1/L} I \end{pmatrix} \quad (37)$$

so that each $A^{(\ell)}$ requires now two qubits to be represented, one physical and one constituting the virtual bond ancillary, plus the dilation ancillary. The virtual bond ancillary must then be initialized and measured in the state $|C\rangle = |R\rangle = |+\rangle$ so that:

$$\bigotimes_{\ell=1}^L (\alpha_\ell I + \beta_\ell X_\ell + \gamma_\ell Y_\ell + \delta_\ell Z_\ell) + \zeta I = \\ (I \quad I) \left[\prod_{\ell=1}^L \begin{pmatrix} \alpha_\ell I + \beta_\ell X_\ell & 0 \\ +\gamma_\ell Y_\ell + \delta_\ell Z_\ell & \zeta^{1/L} I \end{pmatrix} \right] \begin{pmatrix} I \\ I \end{pmatrix}, \quad (38)$$

which lets us identify both preparation gates P_C and P_R with a Hadamard gate. Note that the coefficients $\{\alpha_\ell, \beta_\ell, \gamma_\ell, \delta_\ell\}$ and ζ have been redefined in order to absorb the factor 2 derived by the two Hadamard transformations and the normalization factors that make $\|\mathcal{M}[A^{(\ell)}]\| \leq 1$ for every ℓ .

We have chosen this example due to its simplicity and to test the correct functionality of the entire QET circuit.

E. Eigenstate filtering

Finally, we test our block encoding algorithm, as well as our signal processing technique, by applying an eigenstate filtering function to the Hamiltonian defined in (35). In particular, we want to perform the following transformation over \mathcal{H} [22]:

$$f_d(x, \Delta_\lambda) = \frac{T_d\left(-1 + 2 \frac{x^2 - \Delta_\lambda^2}{1 - \Delta_\lambda^2}\right)}{T_d\left(-1 + 2 \frac{-\Delta_\lambda^2}{1 - \Delta_\lambda^2}\right)} \quad (39)$$

where Δ_λ is the gap between the first and second eigenvalue and T_d is the Chebyshev polynomial of order d . Using the Python package `pyqsp` [3], we have been able to get the angles ϕ_k better approximating the function $f_k(x, \Delta_\lambda)$ through a QET. In figure 7 one can then see a specific example with the Hamiltonian's initial eigenvalues as well as their final values after the entire QET circuit compared with the target filtering function.

`pyqsp` was built for working with quantum signal processing and for acting on a specific one-qubit signal operator, which differs slightly from the conventions that we have used. Still, it is possible to adapt `pyqsp`'s angles for

our purposes by following the instructions in Appendix A.2 of [3].

Moreover, a QET process with these phases generates a complex polynomial transformation, whose real part is our target function. When simulating the circuit, it is therefore necessary to take the hermitian part of the final outcome to get the desired result:

$$\text{poly}(\mathcal{H}) = \frac{1}{2} (f_{\text{QET}}(\mathcal{H}) + f_{\text{QET}}(\mathcal{H})^\dagger). \quad (40)$$

Such a combination of f_{QET} and f_{QET}^\dagger cannot be directly performed on a quantum computer. For simplicity, we leave the question of how to perform this operation on a quantum computer for future work. To demonstrate the working of the algorithm, we have evaluated it classically.

VII. CONCLUSION

Our block encoding method is generally applicable since typical Hamiltonians of interest can be represented as matrix product operators. Moreover, our block encoding technique's computational cost grows only linearly with the system size and quadratically with the virtual bond dimension, offering a potential advantage compared to LCU in terms of one- and two-qubit gate count. In section VI we have shown one specific example of a computational advantage in the case of an exponentially decaying XY model. We remark that our technique uses more ancillary qubits than LCU.

The signal processing operator can have different implementations, as we have shown in section IV, and it incurs a cost growing linearly or quadratically with the number of ancillaries, depending on the chosen implementation and the presence of one extra auxiliary qubit [15, 18].

As previously mentioned, each matrix encoded into a larger unitary must have a bounded norm. Encoding directly \mathcal{H} in a larger unitary, or using LCU, requires $\|\mathcal{H}\| \leq 1$. In our case, we need to normalize each tensor $A^{(\ell)}$ individually, causing an equivalent rescaling of the Hamiltonian by a factor $\prod_{\ell=1}^L N_\ell$. The required renormalization is a general issue of block encoding and is not specific to our MPO approach. We remark that the spectral norms of the individual matrices $\mathcal{M}[A^{(\ell)}]$ are typically easier to calculate than $\|\mathcal{H}\|$. However, $\prod_{\ell=1}^L N_\ell$ can be larger than $\|\mathcal{H}\|$. Note that the final success probability for a QET circuit is not directly impacted by the normalization factor, which appears instead in the polynomial transformation argument, see Eq. (17). Still, an exponential suppression of the eigenvalues might bring some practical disadvantages. We are leaving the question of how to minimize the norms $\|\mathcal{M}[A^{(\ell)}]\|$ for future work.

A possible future project might focus on generalizing our protocol to Hamiltonians defined on two-dimensional lattices and their *projected entangled-pair operator* representation, inspired by isometric tensor networks [23]

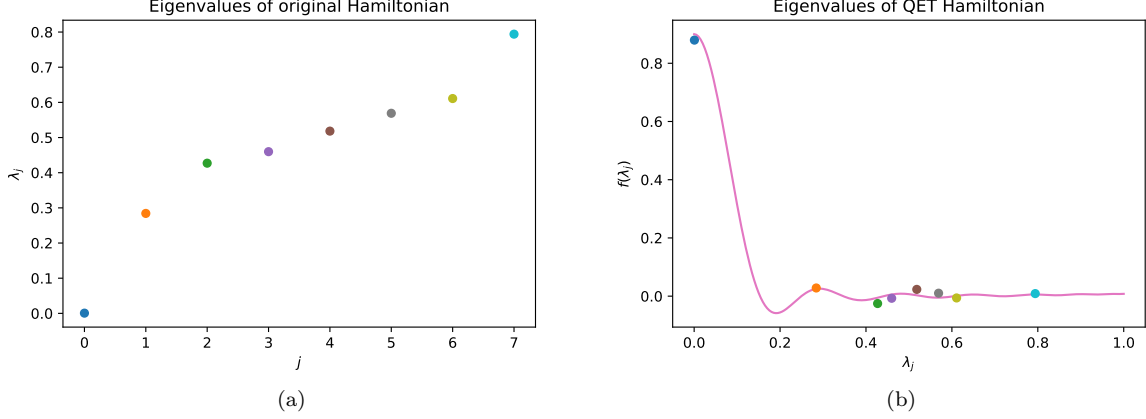


Figure 7. **7a** Original eigenvalues for tensor product of Pauli sums with $L = 3$, $\alpha = \{0.7, 1.2, -0.3\}$, $\beta = \{-1, 0.4, 0.5\}$, $\gamma = \{0, 0.3, 0.5\}$, $\delta = \{0.1, 0, 1.2\}$, $\zeta = 1.7$ and $N = 1.72$. **7b** Filtering function (in pink) plus QET-transformed eigenvalues. Phases were calculated via the `pyqsp` package with degree $d = 30$ and threshold $\Delta_\lambda = 0.1$.

to construct the unitary dilations. This is particularly promising since the qubit topologies of modern quantum computers are often likewise two-dimensional grids.

Our work should then be considered as an introductory publication presenting a new and promising technique, which will need to be further studied in the future, together with other new and interesting applications.

Finally, we acknowledge the existence of a similar work that was made publicly available during the review process of this paper [10], which uses numerical optimizations to find an approximation with reduced effective

bond dimensions.

ACKNOWLEDGEMENTS

M. Nibbi acknowledges funding by the Munich Quantum Valley, section K5 Q-DESSI. The research is part of the Munich Quantum Valley, which is supported by the Bavarian state government with funds from the Hightech Agenda Bayern Plus.

-
- [1] A. Gilyén, Y. Su, G. H. Low, and N. Wiebe, Quantum singular value transformation and beyond: exponential improvements for quantum matrix arithmetics, in *Proceedings of the 51st Annual ACM SIGACT Symposium on Theory of Computing*, STOC 2019 (Association for Computing Machinery, 2019) pp. 193–204.
 - [2] G. H. Low and I. L. Chuang, Hamiltonian simulation by qubitization, *Quantum* **3**, 163 (2019).
 - [3] J. M. Martyn, Z. M. Rossi, A. K. Tan, and I. L. Chuang, Grand unification of quantum algorithms, *PRX Quantum* **2**, 040203 (2021).
 - [4] Y. Kikuchi, C. Mc Keever, L. Coopmans, M. Lubasch, and M. Benedetti, Realization of quantum signal processing on a noisy quantum computer, *npj Quantum Information* **9**, 10.1038/s41534-023-00762-0 (2023).
 - [5] U. Schollwöck, The density-matrix renormalization group in the age of matrix product states, *Ann. Physics* **326**, 96 (2011).
 - [6] M. P. Zaletel, R. S. K. Mong, C. Karrasch, J. E. Moore, and F. Pollmann, Time-evolving a matrix product state with long-ranged interactions, *Phys Rev. B* **91**, 165112 (2015).
 - [7] F. Fröwis, V. Nebendahl, and W. Dür, Tensor operators: Constructions and applications for long-range interaction systems, *Phys. Rev. A* **81**, 10.1103/physreva.81.062337 (2010).
 - [8] G. M. Crosswhite, A. C. Doherty, and G. Vidal, Applying matrix product operators to model systems with long-range interactions, *Phys. Rev. B* **78**, 10.1103/physrevb.78.035116 (2008).
 - [9] S.-H. Lin, R. Dilip, A. G. Green, A. Smith, and F. Pollmann, Real- and imaginary-time evolution with compressed quantum circuits, *PRX Quantum* **2**, 010342 (2021).
 - [10] A. Termanova, A. Melnikov, E. Mamenchikov, N. Belokonev, S. Dolgov, A. Berezutskii, R. Ellerbrock, C. Mansell, and M. Perelshtein, Tensor quantum programming (2024), [arXiv:2403.13486 \[quant-ph\]](https://arxiv.org/abs/2403.13486).
 - [11] A. M. Krol, A. Sarkar, I. Ashraf, Z. Al-Ars, and K. Bertels, Efficient decomposition of unitary matrices in quantum circuit compilers, *Applied Sciences* **12**, 759 (2022).
 - [12] P. Rakyta and Z. Zimborás, Approaching the theoretical limit in quantum gate decomposition, *Quantum* **6**, 710 (2022).
 - [13] M. Saeedi and M. Pedram, Linear-depth quantum circuits for n -qubit toffoli gates with no ancilla, *Physical Review A* **87**, 10.1103/physreva.87.062318 (2013).
 - [14] B. Zindorf and S. Bose, Efficient implementation of multi-controlled quantum gates (2024), [arXiv:2404.02279 \[quant-ph\]](https://arxiv.org/abs/2404.02279).

- [15] R. Vale, T. M. D. Azevedo, I. C. S. Araújo, I. F. Araujo, and A. J. da Silva, Circuit decomposition of multicon-
trolled special unitary single-qubit gates, *IEEE Transactions on Computer-Aided Design of Integrated Circuits and Systems* **43**, 802 (2024).
- [16] A. M. Childs and N. Wiebe, Hamiltonian simulation using
linear combinations of unitary operations, *Quant. Inf. Comput.* **12**, 0901 (2012).
- [17] D. W. Berry, A. M. Childs, R. Cleve, R. Kothari, and
R. D. Somma, Simulating Hamiltonian dynamics with a
truncated Taylor series, *Phys. Rev. Lett.* **114**, 090502
(2015).
- [18] A. J. da Silva and D. K. Park, Linear-depth quantum
circuits for multiqubit controlled gates, *Physical Review A* **106**, 10.1103/physreva.106.042602 (2022).
- [19] M. Plesch and Č. Brukner, Quantum-state preparation
with universal gate decompositions, *Physical Review A* **83**, 10.1103/physreva.83.032302 (2011).
- [20] S.-J. Ran, E. Tirrito, C. Peng, X. Chen, L. T. G. Su, and
M. Lewenstein, *Tensor network contractions - Methods
and applications to quantum many-body systems*, Title
Lecture Notes in Physics (Springer Cham, 2020).
- [21] K. Yamada and K. Fukai, Matrix product operator
representations for the local conserved quantities of
the Heisenberg chain (2023), [arXiv:2306.03431 \[cond-
mat.stat-mech\]](#).
- [22] L. Lin and Y. Tong, Optimal polynomial based quantum
eigenstate filtering with application to solving quantum
linear systems, *Quantum* **4**, 361 (2020).
- [23] M. P. Zaletel and F. Pollmann, Isometric tensor network
states in two dimensions, *Phys. Rev. Lett.* **124**, 037201
(2020).

Appendix A: Signal processing circuit

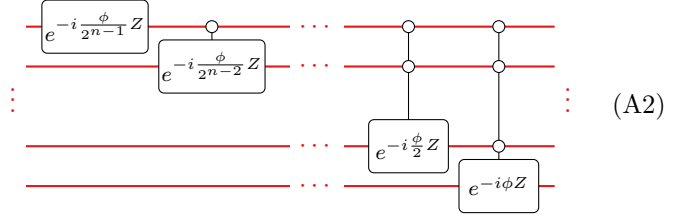
In this section, we prove that the circuits drawn in Eqs. (19) and (18) are equivalent. First of all, we recall the definition of the signal processing operator in Eq. (13). Without loss of generality, we can consider the case in which $|\Pi\rangle = |0\rangle^{\otimes n}$, where n is the total number of ancillary qubits.

The matrix form of Π_ϕ is:

$$\Pi_\phi = \begin{pmatrix} e^{-i\phi} & & & & \\ & e^{i\phi} & & & \\ & & e^{i\phi} & & \\ & & & \ddots & \\ & & & & e^{i\phi} \end{pmatrix}. \quad (\text{A1})$$

It follows directly that Eq. (19) holds, since the state $|0\rangle^{\otimes n}$ is the only one that gains a phase $e^{-i\phi}$, while the other states acquire the phase $e^{i\phi}$.

The general form of our signal processing circuit, without distinguishing between dilation and virtual bond ancillaries, equals:



Let us consider the q -th operator in the circuit (A2). This operator has $q - 1$ controls and a rotation phase of $\frac{-\phi}{2^{n-q}}$. Its matrix expression, considering the tensor multiplication with $n - q$ identities as well, is:

$$\left(\begin{array}{c} \overbrace{\begin{bmatrix} e^{-i\frac{\phi}{2^{n-q}}} & & \\ & \ddots & \\ & & 1 \end{bmatrix}}^{2^{n-q}} \\ \overbrace{\begin{bmatrix} e^{i\frac{\phi}{2^{n-q}}} & & \\ & \ddots & \\ & & 1 \end{bmatrix}}^{2^{n-q}} \\ \overbrace{\begin{bmatrix} 1 & & \\ & \ddots & \\ & & 1 \end{bmatrix}}^{2^{n-q}(2^q-2)} \end{array} \right) \quad (\text{A3})$$

By multiplying all the matrices (A3) with q from 1 to n , we get then the following:

$$\left(\begin{array}{c} \prod_{q=1}^n e^{-i \frac{\phi}{2^{n-q}}} \\ e^{i\phi} \prod_{q=1}^{n-1} e^{-i \frac{\phi}{2^{n-q}}} \\ \overbrace{\left[e^{i \frac{\phi}{2}} \prod_{q=1}^{n-2} e^{-i \frac{\phi}{2^{n-q}}} \right]}^2 \\ \vdots \\ \overbrace{\left[e^{i \frac{\phi}{4}} \prod_{q=1}^{n-3} e^{-i \frac{\phi}{2^{n-q}}} \right]}^4 \\ \vdots \\ \overbrace{\left[e^{i \frac{\phi}{2^{n-1}}} \right]}^{2^{n-1}} \end{array} \right) \quad (\text{A4})$$

Apart from the first entry, we can consider n separate diagonal blocks. Taking $1 \leq k \leq n$, the k -th block has dimension 2^{k-1} and entries equal to $e^{i \frac{\phi}{2^{k-1}}} \prod_{q=1}^{n-k} e^{-i \frac{\phi}{2^{n-q}}}$. We want to prove that each one of these does not depend on k and, more specifically, is equal to $e^{i \frac{\phi}{2^{n-1}}}$:

$$\begin{aligned}
e^{i \frac{\phi}{2^{k-1}}} \prod_{q=1}^{n-k} e^{-i \frac{\phi}{2^{n-q}}} &= e^{i \frac{\phi}{2^{k-1}}} e^{-i\phi \sum_{q=1}^{n-k} \frac{2^q}{2^n}} \\
&= e^{i \frac{\phi}{2^{k-1}}} e^{-i\phi \frac{2-2^{n-k+1}}{2^n(1-2)}} \\
&= e^{i \frac{\phi}{2^{k-1}}} e^{-i\phi \left(\frac{1}{2^{k-1}} - \frac{1}{2^{n-1}} \right)} \\
&= e^{i \frac{\phi}{2^{n-1}}} \quad (\text{A5})
\end{aligned}$$

The first block, on the other hand, has the following entry:

$$\begin{aligned}
\prod_{q=1}^n e^{-i \frac{\phi}{2^{n-q}}} &= e^{-i\phi \sum_{q=1}^n \frac{2^q}{2^n}} \\
&= e^{-i\phi \frac{2-2^{n+1}}{2^n(1-2)}} \\
&= e^{i\phi \left(\frac{1}{2^{n-1}} - 2 \right)} \quad (\text{A6})
\end{aligned}$$

By multiplying both equations (A5) and (A6) by a global phase $e^{i\phi \left(1 + \frac{1}{2^{n-1}} \right)}$ we get then the reference matrix from equation (A1), which proves that the two circuits are equivalent up to a global phase.